Total Variation-based Denoising Model for Bioinformatics Images

Zhenhua Zhou

Xi'an International University
Xi'an, 710077 China
E-mail: 315135305@qq.com

Received: February 17, 2016 **Accepted: November 10, 2016**

Published: December 31, 2016

Abstract: *The total variation-based denoising model enhancement method for bioinformatics images is introduced at the beginning of this paper, and this model morphologically reconstructs and constrains the regularization items. The model is smoothed with variance in different areas by adding the smooth coefficient, and accordingly the image denoising effect is enhanced. Compared with the traditional image filtration model, the optimized total variation-based model is more distinctive in the field of higher items and lower items. As the simulation experiment shows, the optimized total variation-based model has the better effect in denoising. Lastly, by applying the marked-based watershed segmentation algorithm and the optimized total variation-based image denoising model, the bioinformatics image is segmented.*

Keywords: *Denoising model, Bioinformatics image, Total variation model, Image filtration method.*

Introduction

As the most rapidly developing discipline among the bioengineering fields, bioinformatics image processing is a branch of the bioengineering discipline, and mainly consists of biological information processing, biological image processing and analysis. The bioinformatics image analysis is committed to extracting digital information from biological images or biological image sequences. It is widely applied in the field of life sciences [11]. However, a certain amount of noise is normally inevitable within bioinformatics images, and to achieve the follow-up image analysis and process efficiently, the process of denoising for input images shall be enhanced as we seek to optimize the image quality and further pursue the segmentation and location processing. On the one hand, the denoising demand for a bioinformatics image is to both remove the blurring and the noise of the image and preserve all the details of the image, which are the tasks the traditional filtering method fails to accomplish [4]. On the other hand, it is hard to find one suitable segmentation method for bioinformatics images as the images are complex and diverse, and attempts to process and segment the complex bioinformatics images while applying the traditional threshold segmentation method and the marker-driven watershed segmentation algorithm usually fail.

For the past few years, the partial differential equation has been widely applied in each field of the image processing and has led to a series of research results as this theory is widely embraced due to its serious mathematical theory. This paper, aiming at arriving at a better solution for bioinformatics image processing on the basis of the partial differential equation theory, proposes one kind of total variation-based denoising enhanced model suitable for processing bioinformatics images given that the total variation-based model is susceptible to noise and loses important and detailed information while processing images [6].

The regularization terms are enhanced as the regularization items are constrained by applying morphological reconstruction a priori knowledge. The marginal texture of bioinformatics images gets strengthened through adding a new accommodation coefficient for smooth items. As the model analysis and the experimental result show, the proposed total variation-based model is superior to the traditional model in the field of denoising [8]. The model discussed hereof can also be applied for effectively preprocessing images as they are. The target area of bioinformatics images can be efficiently grasped by combining the total variation-based model and the marker-driven watershed segmentation algorithm.

Materials and methods

Variation method theory

Set $F\left(x, y(x), y`(x)\right)$ as the known function for three independent variables, $x, y(x)$, $y`(x)$ in the $[x_0, x_1]$ interval, and the function is continuously differentiable in the second phase. $y(x), y`(x)$ are the unknown function of *x*. The functional is demonstrated as follows:

$$J\left[y(x)\right] = \int_{x_0}^{x_1} F\left(x, y(x), y`(x)\right) dx. \tag{1}$$

This functional hereof is called the most simple functional.

The functional $J\left[y(x)\right]$ is called the functional form or the variation integral, and the integrand *F* is called the kernel of the functional, variation integral function or the Lagrange function.

It can be known from the above formula that $J\left[y(x)\right]$ is not merely the function of $y(x)$, but also the function of *x* and $y`(x)$. As long as $y(x)$ is calculated, the $y`(x)$ can also be calculated.

In the first phase of $y = y(x)$, select any curve from $y = y_1(x)$, there is:

$$\delta y = y_1(x) - y(x),\ \delta`y = y`_1(x) - y`(x). \tag{2}$$

The increment of the most simple functional $J\left[y(x)\right]$ is:

$$\begin{aligned} \Delta J &= J\left[y_1(x)\right] - J\left[y(x)\right] = J\left[y(x) + \delta y\right] - J\left[y(x)\right] \\ &= \int_{x_0}^{x_1} F\left(x, y + \delta y, y`, \delta`y\right) dx - \int_{x_0}^{x_1} F\left(x, y, y`\right) dx \\ &= \int_{x_0}^{x_1} \left[F\left(x, y + \delta y, y`, \delta`y\right) - F\left(x, y, y`\right)\right] dx. \end{aligned} \tag{3}$$

The increment of the functional is also called the total variation of the functional.

On the basis of the Taylor mean value theorem of function of two variables, the following formula is available:

$$F\left(x, y, +\delta y, y`+\delta`y\right)-F\left(x, y, y`\right)=\overline{F}_{y}\delta y+\overline{F}_{y`}\delta y`. \tag{4}$$

According to the above formula, the $\overline{F}_{y}$ and $\overline{F}_{y`}$ are recognized as the values of $F_y$ and $F_{y`}$ respectively in the interval of $\left(x, y(x), y`(x)\right)$. The value of $\overline{y}(x)$ is between $y(x)$ and $y_1(x)$. $\overline{y}`(x)$ is between $y`(x)$ and $y`_1(x)$.

$$\begin{aligned}&\left|\overline{y}(x)-y(x)\right|<d_1\left[y_1(x), y(x)\right],\\&\left|\overline{y}`(x)-y`(x)\right|<d_1\left[y_1(x), y(x)\right].\end{aligned} \tag{5}$$

For any value $\varepsilon_1>0$, $\varepsilon_2>0$, when $d_1\left[y_1(x), y(x)\right]$ is sufficiently low, the following value is definitely available:

$$\left|\overline{F}_{y}-F_{y}\right|<\varepsilon_1, \left|\overline{F}_{y`}-F_{y`}\right|<\varepsilon_2. \tag{6}$$

Thus, it is available that:

$$\Delta J=\int_{x_0}^{x_1}\left(\overline{F}_{y}\delta y-\overline{F_{y`}}\delta y`\right)dx=\int_{x_0}^{x_1}\left(F_y\delta y-F_{y`}\delta y`\right)dx+\varepsilon d_1\left[y_1(x), y(x)\right]. \tag{7}$$

Among the above formula,

$$\varepsilon d_1\left[y_1(x), y(x)\right]=\int_{x_0}^{x_1}\left[\left(\overline{F}_{y}-F_{y}\right)\delta y+\left(\overline{F}_{y`}-F_{y`}\right)\delta y`\right]dx \tag{8}$$

and ε approaches zero as $d_1\left[y_1(x), y(x)\right]$ approaches zero.

If functional (1) is continuous in the second phase, and its increment can be indicated as $\Delta J=L\left[y(x), \delta y\right]+d\left[y(x), \delta y\right]$. The $d\left[y(x), dy\right]$ hereof is the high order infinitesimal of δy, and accordingly the functional hereof is differentiable in the function of $y=y(x)$.

$$\begin{aligned}\delta J&=\int_{x_0}^{x_1}\left[\left(\overline{F}_{y}-F_{y}\right)\delta y+\left(\overline{F}_{y`}-F_{y`}\right)\delta y`\right]dx\\&=\int_{x_0}^{x_1}\left(F_y\delta y+F_{y`}\delta y`\right)dx\\&=\int_{x_0}^{x_1}\left(F_y\varepsilon\eta+F_{y`}\varepsilon\eta`\right)dx\\&=\varepsilon\int_{x_0}^{x_1}\left(F_y\eta+F_{y`}\eta`\right)dx.\end{aligned} \tag{9}$$

Theorem: When $J\left[y(x)\right]$ acquires extremum in the function of $y=y(x)$, the variation δJ in the function of $y=y(x)$ equals zero. δJ = 0, the variation of $J\left[y(x)\right]$ is the essential condition of functional extremum and the variation principle [21].

The variation can be changed into an exclusive δy linear function under the sig of integration through adapting integration by parts, which is called the Lagrange variation. The Lagrange variation is demonstrated as follows.

The following value is available by applying integration by parts for the second item under the sign of integration of the above formula:

$$\int_{x_0}^{x_1} F_{y`}\delta y`dx = F_{y`}\delta y\Big|_{x_0}^{x_1} - \int_{x_0}^{x_1} \delta y \frac{d}{dx}F_{y`}dx . \tag{10}$$

If the variation value at the points x_0 and x_1 equals zero, then,

$$\int_{x_0}^{x_1} F_{y`}\delta y`dx = -\int_{x_0}^{x_1} \delta y \frac{d}{dx}F_{y`}dx . \tag{11}$$

Thus,

$$\delta J = \int_{x_0}^{x_1} \left(F_{y`}\delta y + F_{y`}\delta y`\right)dx = \int_{x_0}^{x_1} \left(F_y - \frac{d}{dx}F_{y`}\right)\delta y dx . \tag{12}$$

Theorem: Allowing the most simple functional

$$J\left[y(x)\right] = \int_{x_0}^{x_1} F\left(x, y(x), y`(x)\right)dx . \tag{13}$$

Acquire the extremum and meeting the fixed edge condition

$$y(x_0) = y_0,\ y(x_1) = y_1 . \tag{14}$$

The extreme curve $y = y(x)$ shall meet the essential condition

$$F_y - \frac{d}{dx}F_{y`} = 0 . \tag{15}$$

The F within is the known function of $\left(x,\ y(x),\ y`(x)\right)$ and has partial derivative continuing in the second phase. The above formula is also called the Euler-Lagrange equation.

Total variation model

The basic theory of bounded variation function space provides the theoretical basis for image processing and low-level visual analysis on the basis of the variation method and PDE [20]. The BV space is regarded as the relatively reasonable function space for non-texture images. The total variation is the classical model for processing images and demonstrates the practical effect of the BV space theory [5].

The total variation model is proposed jointly by Rudin, Osher and Faterni, and has become the most successful model for denoising and restoring images. The main advantage of this

model lies in its ability to preserve the edge features of images while denoising them at the same time.

Set *u* as the original image, f as the noised image, u_0 as the signal of noise, and the following formula is available:

$$f(x,y)=u(x,y)+u_0(x,y). \tag{16}$$

According to the theory of the total variation model, the total variation of noise images is relatively more obvious than the total variation of noiseless images. Thus, minimizing the effect of total variation can effectively denoise. The minimized total variation is indicated by the following formula:

$$\min\left(\int_{\Omega}|\nabla u|\,d\Omega\right)=\min\left(\int_{\Omega}\sqrt{\left(\frac{\partial u}{\partial x}\right)^2+\left(\frac{\partial u}{\partial y}\right)^2}\,dxdy\right). \tag{17}$$

Results and discussion

The success of the total variation-based model is that, on the basis of the inner regularity of images, the model can reveal the actual smoothness on the edge of an image through the solution of noise images. This process is specifically realized by introducing the energy function and turning the task of denoising images into a process of seeking the minimum of a functional.

The total variation method can be easily realized. However, as the model detects the edge by applying gradient information, it is easily susceptible to noise, and the important and detailed information might be lost during the image processing [2]. The fundamental purpose of denoising bioinformatics images is to make the processed bioinformatics images more effective and adequate to be further applied. To demonstrate this point more specifically, background impurity shall be eradicated, too much noise is not allowed, detailed distortion shall not be caused and the edge definition, contour and contrast ratio of an image shall be optimized while denoising the image [14]. To meet the requirements of denoising bioinformatics images, the total variation-based enhanced denoising model is proposed.

According to the TV theory, $\int_{\Omega}\nabla u|dxdy$ is the parameter of the smooth item, and its energy function can be rewritten. This paper initially replaces the u image by the *Mu* image reconstructed by morphological opening and closing and eradicates the smaller bright points and dark points, achieves smoothness by removing bug dots and fills the contour gap by applying morphological opening and the closing reconstruction algorithm [7, 16, 17]. Accordingly, the edge is smooth and the details of the image are optimized and perfected. There are two benefits gained in the wake of this process. Firstly, a part of the noise can be removed and consequently the impact of the noise on the edge gradient is reduced. Secondly, in the field of data preservation and fidelity, the data approach the original more closely and the denoising effect can be enhanced [1, 3, 13, 15, 18].

The modified total variation model can be defined as follows:

$$\min\left(\int_{\Omega}\left|\nabla Mu\right|dxdy+\frac{\lambda}{2}\int_{\Omega}\left(Mu-f\right)^{2}dxdy\right). \tag{18}$$

In view of the modified formula, the first item is the regularization parameter of the smooth image, and the second item is the functional precision used for distinguishing *Mu* and *f*. λ is the Lagrange's multiplier used for balancing the said two items of the model [22].

Further, to achieve the automatic adjustment of the regularization parameter of the smooth image according to different gradients, the adjustable parameter is added for the first item of the model. The optimized total variation denoising model for the image is defined as follows:

$$\min\left(\left(1+\frac{1}{1+\left|\nabla Mu\right|^{2}}\right)\int_{\Omega}\left|\nabla Mu\right|dxdy+\frac{\lambda}{2}\int_{\Omega}\left(Mu-f\right)^{2}dxdy\right). \tag{19}$$

As for the smooth item parameter, set $\gamma=1+\frac{1}{1+\left|\nabla Mu\right|^{2}}$. The range of γ is [1, 2), and there is $\left|\nabla Mu\right|\to\infty$ approaching to the edge. At this time, γ = 1, and the smooth item parameter reaches its minimum. However, there is $\left|\nabla Mu\right|\to 0$ in the flat areas, and γ = 2. Then select a relatively bigger smooth parameter to achieve image smoothing. Thus, the total variation parameters can be adjusted automatically by the new model according to different gradients, as we seek to reach the goal of both denoising and preserving edge details [12].

Set

$$F\left(Mu,\nabla Mu\right)=\frac{\lambda}{2}\left(Mu-f\right)^{2}+\left(1+\frac{1}{1+\left|\nabla Mu\right|^{2}}\right)\left|\nabla Mu\right|. \tag{20}$$

The Euler-Lagrange equation for Eq. (25) is as follows:

$$F_{Mu}-\frac{d}{dx}\left\{Fp\right\}-\frac{d}{dy}\left\{Fq\right\}=0. \tag{21}$$

Among the equations,

$$p=\frac{\partial Mu\left(x,y\right)}{\partial x},\ q=\frac{\partial Mu\left(x,y\right)}{\partial y} \tag{22}$$

and

$$F_{Mu}=\frac{\partial F}{\partial Mu}=\lambda\left(Mu-f\right), \tag{23}$$

$$F_p = \left(1+\left(\frac{1}{1+|\nabla Mu|^2}-2|\nabla Mu|\frac{|\nabla Mu|}{|\nabla Mu|^2}\right)\right)\frac{\frac{\partial Mu}{\partial x}}{|\nabla Mu|}$$
$$=\left(\frac{1}{1+|\nabla Mu|^2}-1\right)\frac{\frac{\partial Mu}{\partial x}}{|\nabla Mu|}, \tag{24}$$

$$F_q = \left(1+\left(\frac{1}{1+|\nabla Mu|^2}-2|\nabla Mu|\frac{|\nabla Mu|}{|\nabla Mu|^2}\right)\right)\frac{\frac{\partial Mu}{\partial y}}{|\nabla Mu|}$$
$$=\left(\frac{1}{1+|\nabla Mu|^2}-1\right)\frac{\frac{\partial Mu}{\partial y}}{|\nabla Mu|}. \tag{25}$$

The following derivations are available by plugging Eqs. (24), (25) into Eq. (23):

$$\lambda(Mu-f)-\left(\frac{1}{1+|\nabla Mu|^2}-1\right)\left(\frac{\partial}{\partial x}\left(\frac{\frac{\partial Mu}{\partial x}}{|\nabla Mu|}\right)+\frac{\partial}{\partial y}\frac{\frac{\partial Mu}{\partial y}}{|\nabla Mu|}\right)=0, \tag{26}$$

$$\Rightarrow \lambda(Mu-f)-\left(\frac{1}{1+|\nabla Mu|^2}-1\right)\left(\frac{\partial}{\partial x},\frac{\partial}{\partial y}\right)\left(\frac{\frac{\partial Mu}{\partial x}}{|\nabla Mu|},\frac{\frac{\partial Mu}{\partial y}}{|\nabla Mu|}\right)=0,$$
$$\Rightarrow \lambda(Mu-f)-\left(\frac{1}{1+|\nabla Mu|^2}-1\right)\left(\frac{\partial}{\partial x},\frac{\partial}{\partial y}\right)\frac{1}{|\nabla Mu|}\left(\frac{\partial Mu}{\partial x},\frac{\partial Mu}{\partial y}\right)=0, \tag{27}$$
$$\Rightarrow -\nabla\left(\frac{\nabla Mu}{|\nabla Mu|}\left(\frac{1}{1+|\nabla Mu|^2}-1\right)\right)+\lambda(Mu-f).$$

Experiment and result

To verify the effect of the optimized model for denoising bioinformatics images as proposed, a simulation experiment is conducted. This paper selects cell images and MRI images as subjects and compares the denoising effect among classical partial differential equation denoising models, including the PM model, Lin Shi model, TV model and the model proposed and discussed in this paper. The subjects of cell images come from the Internet, and the MRI images have been taken from the radiology department of a hospital [19]. Fig. 1 compares the results of the denoising effect for biological cell images under different models. Fig. 1a) displays a cell image with 50% Gaussian noise. It is made clear in this paper that the model proposed hereof successfully removes most of the noise and better preserves the edge of the cell compared with other PDE model denoising results.

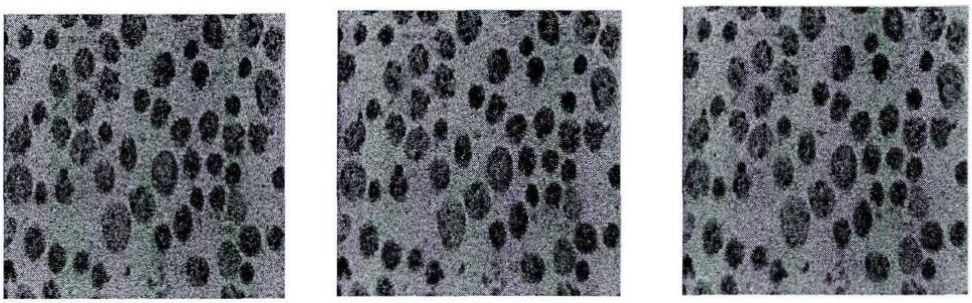

a) Noised image b) PM model c) Lin Shi model

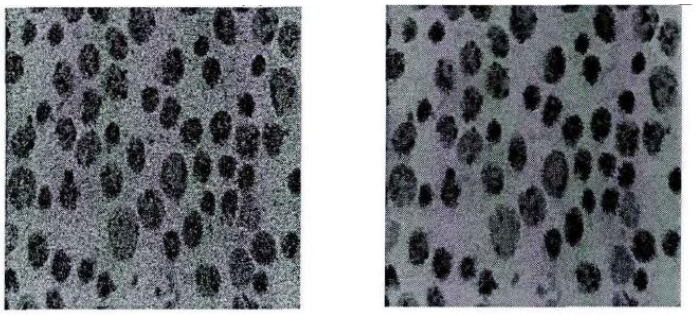

d) TV model e) Proposed model

Fig. 1 Cell result images of different denoising models

Fig. 2 illustrates the enhanced results for optimizing cell images conducted by applying the model proposed hereof. The original Fig. 2a inevitably contains a certain amount of noise, which brings difficulties for separating and extracting cells in the following process. Fig. 2b shows that the noise within the background image is eradicated by applying the TV model proposed in this paper, and the edge of the cell is preserved, which lays a favorable foundation for further processing.

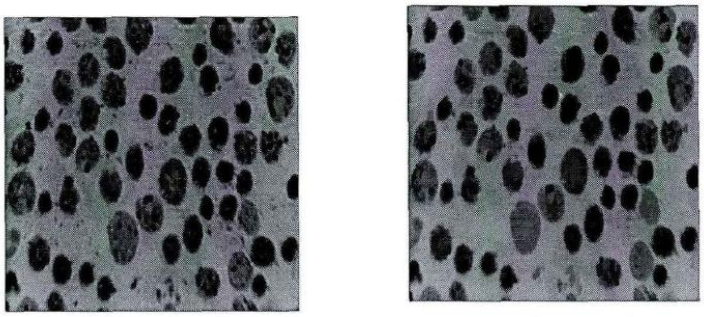

a) Original image b) Result image

Fig. 2 Cell result images of modified TV denoising model

Fig. 3 illustrates the denoising effects of applying different models. Fig. 3a is a cell image containing 20% of Gaussian noise. The first line of the figure indicates the denoising effects of applying different models, and the second line refers to the partial enlarged details of the first line. As these data show, the model proposed in this paper can eradicate most of the noise and preserve the edge definition of kidney.

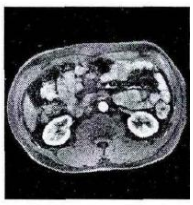
a) Noised image

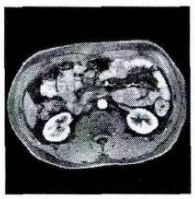
b) PM model

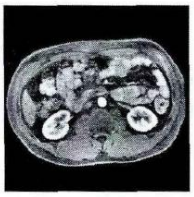
c) Lin Shi model

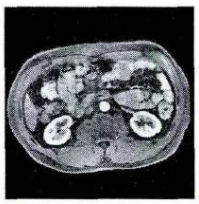
d) TV model

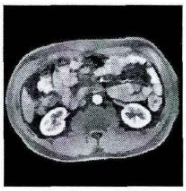
e) Proposed model

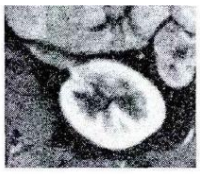
f) Sub-region of a)

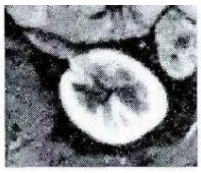
g) Sub-region of b)


h) Sub-region of c)

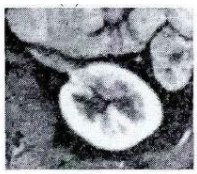
i) Sub-region of d)

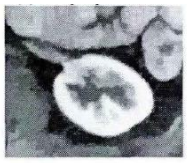
j) Sub-region of e)

Fig. 3 MRI result images of different denoising models

By viewing the above figures of the experiment result, it can be directly grasped that the new proposed optimization-based TV model has a favorable effect on denoising bioinformatics images. It not only eradicates the noise, but also strengthens the edge definition of an image. Consequently, the model lays a favorable foundation for further processing the image [10]. Similarly, to further demonstrate the superiority of this algorithm, this paper applies PSNR (peak signal to noise ratio) and NMSE (normalized mean square error) as the standard for measuring the effectiveness of denoising different models [9]. The bioinformatics images and noise ratios by applying each PDE model mentioned in the cell images of Fig. 2 are displayed in Table 1. It can be seen from the table that the modified total variation-based model has superior performance in the field of processing bioinformatics images, and the PSNR value of the proposed model is higher than the traditional partial differential equation model. Especially the proposed model has better effects as the ratio of noise is increasing. Table 2 illustrates the PSNR values for the TV denoising model under different ratios of Gaussian noise of MRI images displayed in Fig. 3. It is clear that the PSNR of the new model increases at a percentage of more than 40% compared with the traditional TV model.

Table 1. PSNR of different denoising models with white Gaussian noise

Gaussian variance	Signal to noise ratio	The PM model	Lin Shi model	TV model	The proposed model
0.01	PSNR	23.52	24.25	25.147	26.54
0.01	NMSE	1.236	1.245	0.6585	0.365
0.02	PSNR	18.45	20.65	21.658	21.84
0.02	NMSE	0.355	0.358	0.5477	0.301
0.03	PSNR	13.26	14.58	15.269	19.26
0.03	NMSE	1.524	1.284	0.9254	0.412

Table 2. PSNR of two different TV models with white Gaussian noise

Gaussian variance	TV model	The proposed model	Rise rate
0.02	15.245	22.854	44.15%
0.04	11.236	19.325	73.25%

Bioinformatics image segmentation method on the basis of total variation and marked-based watershed segmentation algorithm

As the traditional marked-based watershed segmentation can lead to over-segmentation, a number of scholars have proposed corresponding solutions. Some classical solutions proposed are to resolve the over-segmentation by applying marking and hierarchy. The marking can be the gray value or complex properties like size, shape, location, distance and texture information. The segmentation can be more precise by increasing a priori knowledge through applying this method. This paper adapts the marked-based watershed segmentation algorithm proposed by Soille. The specific process is to firstly set the foreground marking and background marking on the image, the former corresponds to the target image, and the latter corresponds to the background image. Secondly, these two markings are morphologically reconstructed as the minimum of the gradient image. Lastly, the marked-based watershed segmentation is processed.

This paper applies multi-scale morphology structural elements and adapts dual discoid structure elements with different radiuses, and consequently an adequate gradient image can be acquired and the original edge definition preserved. Fig. 4a of Fig. 4 is the original image, Fig. 4b is the morphological gradient image and Fig. 4c is the multi-scale morphological gradient image. It is clear that the maximum gradient value is continuous on the edge of Fig. 4c, and the edge definition information of the original image can be clearly reflected. When marking the foreground and background images, this paper adapts the OTSU method to mark the images and classify them as target images or background images.

To verify the effectiveness of combining the optimized total variation-based enhanced denoising model and the marked-based watershed segmentation for extracting the edge definition of bioinformatics images, experiments with biological cell images and biological MRI images have been conducted. Fig. 5 illustrates the results of biological cell images following the mentioned segmentation method. Fig. 5h displays the result of directly adapting

the marked-based watershed segmentation algorithm on the basis of Fig. 5a. Fig. 5g shows the segmentation result of the proposed method. By comparing these two results, it can be grasped that the proposed method is relatively more effective. As the edge definition is enhanced and optimized after being denoised by applying the TV model, more accurate cell edge images can be segmented.

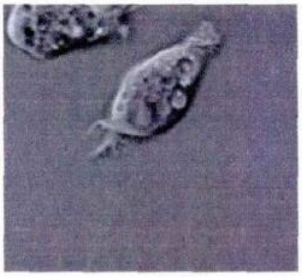

a) Original image

b) Morphological gradient image

c) Multi-scale morphological gradient image

Fig. 4 Morphological gradient images

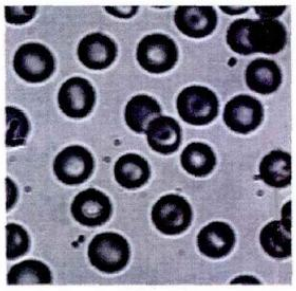

a) Original image

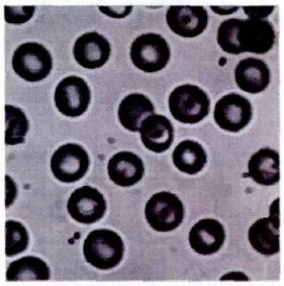

b) Result image after the proposed model

c) Foreground marker image

d) Background marker image

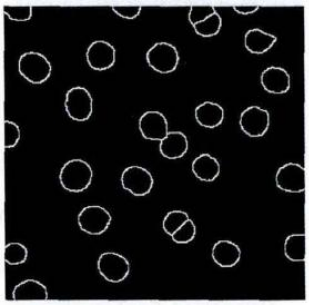

e) Imposed minimum morphological gradient image

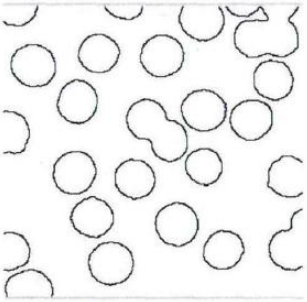

f) Watershed transformation of e)

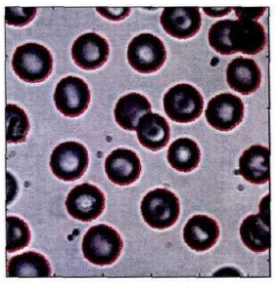

g) Result image

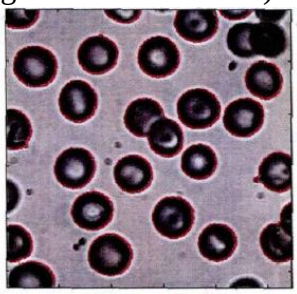

h) Segmentation on a)

Fig. 5 Cell result images of watershed segmentation

Fig. 6 illustrates the results of kidney MRI images following the mentioned segmentation method. The experimental results show that the bioinformatics image segmentation method combined with the optimized total variation-based enhanced denoising model and the marked-based watershed segmentation yield a higher performance in segmenting.

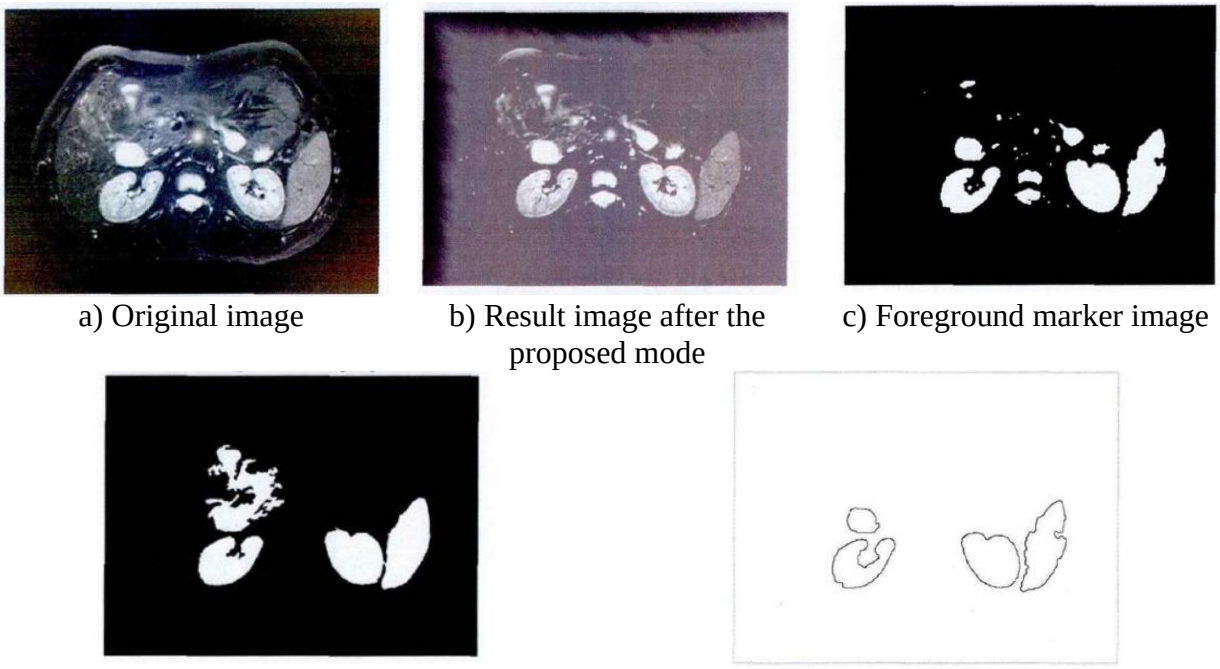

a) Original image b) Result image after the proposed mode c) Foreground marker image

d) Background marker image e) Watershed transformation result

Fig. 6 MRI result images of watershed segmentation

Conclusion

The optimized total variation-based enhanced denoising model has been introduced and analyzed, and the edge definition image has been enhanced by applying automatic smooth parameters. Research shows that the optimized total variation-based enhanced denoising model is superior to the traditional image filtration model in denoising, and the marked-based watershed segmentation algorithm can effectively extract the target area of bioinformatics images.

References

1. Achim A. M., P. Tsakalides, A. Bezerianos (2003). Sar Image Denoising via Bayesian Wavelet Shrinkage Based on Heavy-tailed Modeling, IEEE Transactions on Geoscience and Remote Sensing, 41(8), 1773-1784.
2. Beck A., M. Teboulle (2009). Fast Gradient-based Algorithms for Constrained Total Variation Image Denoising and Deblurring Problems, IEEE Transactions on Image Processing, 18(11), 2419-2434.
3. Bhoi A. K., K. S. Sherpa, B. Khandelwal (2015). Multidimensional Analytical Study of Heart Sounds: A Review, International Journal Bioautomation, 19(3), 351-376.
4. Buades A., B. Coll, J. M. Morel (2005). A Review of Image Denoising Algorithms, with a New One, SIAM Journal on Multiscale Modeling & Simulation, 4(2), 490-530.
5. Chang S. G., B. Yu, M. Vetterli (1998). Spatially Adaptive Wavelet Thresholding with Context Modeling for Image Denoising, IEEE Transactions on Image Processing, 9(9), 1522-1531.

6. Chang S. G., B. Yu, M. Vetterli (2000). Adaptive Wavelet Thresholding for Image Denoising and Compression, IEEE Transactions on Image Processing, 9(9), 1532-1546.
7. Chen T., K. K. Ma, L. H. Chen (1999). Tri-state Median Filter for Image Denoising, IEEE Transactions on Image Processing, 8(12), 1834-1838.
8. Dabov K., A. Foi, V. Katkovnik, K. Egiazarian (2007). Image Denoising by Sparse 3D Transform-domain Collaborative Filtering, IEEE Transactions on Image Processing, 16(8), 2080-2095.
9. Dong W., X. Li, L. Zhang, G. Shi (2011). Sparsity-based Image Denoising via Dictionary Learning and Structural Clustering, IEEE Conference on Computer Vision & Pattern Recognition, 42(7), 457-464.
10. Elad M., M. Aharon (2006). Image Denoising via Learned Dictionaries and Sparse Representation, 2006 IEEE Computer Society Conference on Computer Vision and Pattern Recognition, 1(1), 895-900.
11. Elad M., M. Aharon (2006). Image Denoising via Sparse and Redundant Representations over Learned Dictionaries, IEEE Transactions on Image Processing, 15(12), 3736-3745.
12. Katkovnik V., A. Foi, K. Egiazarian, J. Astola (2010). From Local Kernel to Nonlocal Multiple-model Image Denoising, International Journal of Computer Vision, 86(1), 1-32.
13. Kervrann C., J. Boulanger (2006). Optimal Spatial Adaptation for Patch-based Image Denoising, IEEE Transactions on Image Processing, 15(10), 2866-2878.
14. Kivanc M. M., I. Kozintsev, K. Ramchandran, P. Moulin (1999). Low-complexity Image Denoising Based on Statistical Modeling of Wavelet Coefficients, IEEE Signal Processing Letters, 6(12), 300-303.
15. Luisier F., T. Blu (2008). Sure-let Multichannel Image Denoising: Interscale Orthonormal Wavelet Thresholding, IEEE Transactions on Image Processing, 17(4), 482-492.
16. Luisier F., T. Blu, M. Unser (2007). A New Sure Approach to Image Denoising: Interscale Orthonormal Wavelet Thresholding, IEEE Transactions on Image Processing, 16(3), 593-606.
17. Moulin P., J. Liu (1999). Analysis of Multiresolution Image Denoising Schemes Using Generalized Gaussian and Complexity Priors, IEEE Transactions on Information Theory, 45(3), 909-919.
18. Pizurica A., W. Philips (2006). Estimating the Probability of the Presence of a Signal of Interest in Multiresolution Single- and Multiband Image Denoising, IEEE Transactions on Image Processing, 15(3), 654-65.
19. Pizurica A., W. Philips, I. Lemahieu, M. Acheroy (2002). A Joint Inter- and Intrascale Statistical Model for Bayesian Wavelet Based Image Denoising, IEEE Transactions on Image Processing, 11(5), 545-557.
20. Portilla J., V. Strela, M. J. Wainwright, E. P. Simoncelli (2003). Image Denoising Using Scale Mixtures of Gaussians in the Wavelet Domain, IEEE Transactions on Image Processing, 12(11), 1338-1351.
21. Starck J. L., E. J. Candès, D. L. Donoho (2002). The Curvelet Transform for Image Denoising, IEEE Transactions on Image Processing, 11(6), 670-684.
22. Zhang L., W. Dong, D. Zhang, G. Shi (2010). Two-stage Image Denoising by Principal Component Analysis with Local Pixel Grouping, Pattern Recognition, 43(4), 1531-1549.

Zhenhua Zhou, M.Sc.
E-mail: 315135305@qq.com

Zhenhua Zhou is a lecturer with Master degree. He obtained his Bachelor's degree in Electronic and Information Engineering from Xi'an International University in 2010 and his Master's degree in Software Engineering from University of Electronic Science and Technology of China in 2014. Since 2010, he has been a teacher of Xi'an International University. His research interests include computer application technology, computer virtual 3D image production, 3D simulation virtual reality, computer graphics image processing and postproduction of the film and television.